TUMOR THERAPY WITH HEAVY CHARGED PARTICLES

G. Kraft

Biophysik, Gesellschaft für Schwerionenforschung,
Planckstr. 1, 64291 Darmstadt, Germany

ABSTRACT

The inverse depth dose profile i.e. the increase of the dose with penetration depth make heavy charged particles like protons and heavy ions an ideal tool for the radiotherapy of deep-seated tumors. For carbon ions this good dose profile is potentiated by an additional increase in the relative biological effectiveness (RBE) towards the end of the particle range. The physical and biological basis of the action of ion beams in cells and tissues is briefly reviewed and the variation of radiobiological effectiveness as function of the radiation quality will be explained. The different technical solutions for the shaping of the radiation area according to the planned target volume are presented. The possibility to monitor *in situ* the area affected by the beam in the patient by means of positron emission tomography PET is illustrated. Different layouts of therapy units are compared for protons and carbon ions. Finally, the long way from the first proposal for a medical application of ion beams to the current situation is summarized. Because of the clinical success of ion beam treatment all further centers are planned all over the world.

Contents List

I INTRODUCTION

Shortly after the discovery by W.C. Roentgen in 1895, X-rays were also applied in therapy of malignant tissue. Because their nature and their biological interaction were not known at that time, X-rays were first used on a very empirical basis. The first therapy trial is reported by Prof. Freund in Vienna who irradiated and removed a hairy mole on the forearm of a patient [Hall 1994]. For a long time radiation therapy remained a more or less empirical science where the major progress originated from clinical application although laboratory research widened the scientific horizon dramatically. In the historical development of radiotherapy two general tendencies are visible: the clinical results are improved by a greater conformity of the applied radiation to the target volume and by an increased biological effectiveness of the radiation [Wambersie 1989].
In order to overcome the limitations of an exponentially decreasing depth dose distribution of electromagnetic radiation and in order to improve the lateral beam scattering, numerous techniques have been developed and applied. To reduce the dose to the healthy tissue in front of the target volume, the energy of the photon was increased for the treatment of deep-seated tumors. The originally used X-ray tubes were replaced by high-energy gamma rays, after ^{60}Co sources could be produced in nuclear reactors. Presently, an intensity-modulated distribution of electron bremsstrahlung of high-energy electron linacs yields excellent dose distributions when applied from several directions. In other techniques, radioactive sources of low range emitters are implanted directly into the tumor to achieve a target-conform exposure. Intra-operative irradiation also tries to spare healthy tissue while maximizing the tumor dose at the same time. In general, all these techniques yielded better clinical results when the tumor was exposed to a greater dose without increasing the dose delivered to the normal tissue.

The second tendency was to selectively increase the biological effectiveness of the radiation dose delivered to the tumor. Because some tumors contain hypoxic cells that are up to three times more radioresistant than the corresponding oxygenated cells, major effort was put in decreasing the radio-tolerance of hypoxic cells by hypoxic sensitisers or by the exposure to hyperbaric oxygen pressure. Both methods, however, fell short of expectations. A local hyperthermia of the tumor in order to improve its radiation response is still under research but so far is has not resulted in a major breakthrough in the treatment of radioresistant tumors. The radiobiological rationale for these treatment procedure is given for instance by Hall [Hall 1994].

Finally, electromagnetic radiation has also been replaced by beams of different biological interaction mechanisms. In these trials neutrons and negative pions were applied. For the pions an increase in dose due to the nuclear reaction the “star formation” at the end of the range was expected as well as an increase of the biological effectiveness. Worldwide trials could not meet these expectations in the clinical results and pion therapy was stopped altogether after the treatment of approximately 1,200 patients. For neutrons the increase in biological effectiveness could be translated into a better tumor control but because of the poor depth dose profile this advantage was mostly compensated by severe late effects in the normal tissue. Presently, therapy with low-energy neutrons has mostly phased out but high-energy neutrons and boron neutron capture are still subjects of clinical interest [Wambersie 1995].

In order to overcome the physical and biological limitations of the conventional radiotherapy the use of heavy-charged particles like protons or heavier ions was proposed. In a first paper Robert Wilson has investigated the depth dose profile of protons produced at the Berkeley cyclotron and observed a steep increase of energy deposition i.e. of dose at the end of the particle range [Wilson 1946]. This increase in ionization density had been measured in 1903 for alpha particles by Bragg and is known as Bragg profile. It is very evident that the increase in ionization density towards the end of the particle track allows to transport a higher dose to a deep-seated tumor than would be possible using conventional photon beams (Fig. 1). As turned out in practice of particle therapy the small lateral scattering of heavy particles as well as the restricted range i.e. the steep decrease in

dose beyond the Bragg maximum are the essential properties of particle beams to improve radiotherapy. In addition, at a microscopic scale the increase in ionization density towards the end of the particle range causes an increase of biological effectiveness for ions heavier than protons that can be used to potentiate the radiation damage selectively in the target volume when using the appropriate species like carbon ions [Kraft 1990].

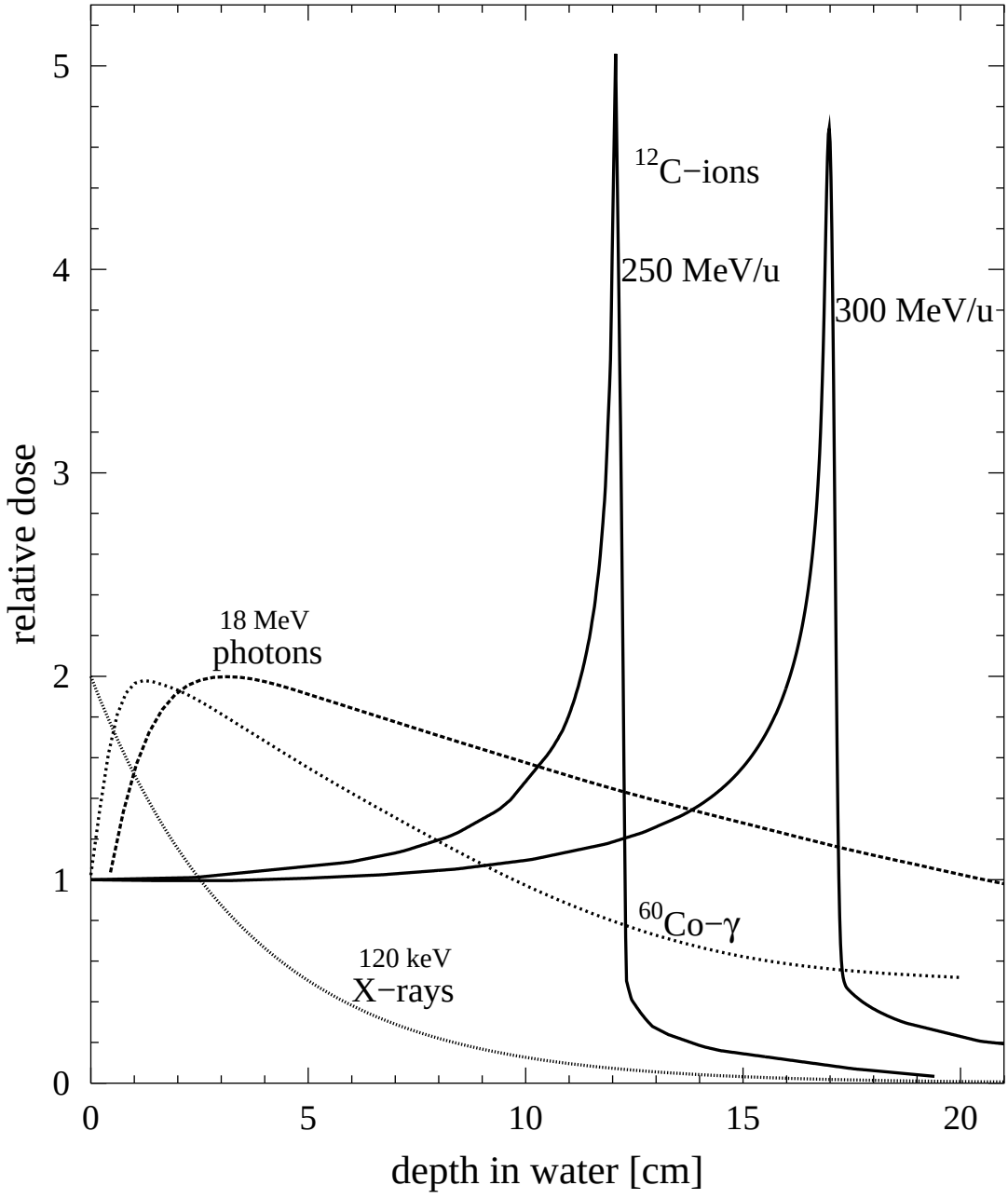

Fig. 1 Comparison of the depth dose profiles of X-rays, Co-gamma and Röntgen-Bremsstrahlung with carbon ions of 250 MeV/u and 300 MeV/u [with the courtesy of U.Weber].

In general, the transition from electromagnetic radiation to heavy-charged particles represents a quantum jump regarding conformity and effectiveness of the applied radiation dose, but it also requires new techniques of beam application and treatment planning in order to ensure that the extremely efficient part of the beam is restricted to the tissue that is to be destroyed and spares the normal tissue around [Raju 1980].

One essential prerequisite for such a conformal treatment is the correct knowledge of the position of the tumor inside the patients' body. Only the development of 3-dimensional imaging, first realized in computerized tomography (CT), provides the necessary information with sufficient precision. Frequently, this information has to be augmented by magnetic resonance imaging (MRI) and positron emission tomography (PET) in order to differentiate between malignant and non-malignant tissue. This is necessary to correctly delineate the 3-dimensional contours of the target volume to be irradiated. There, the development of beam application paralleled the improvement in diagnostic resolution.

From the first proposal of Robert Wilson [Wilson 1996] to the very sophisticated beam delivery by scanning techniques of today it was a long way of research and development, that is based on the improvement in many different areas like accelerator control, fast position-sensitive detectors from high energy physics as well as the progress in particle radiobiology.

In the first trials at Berkeley, beam application methods have been developed that were adapted from conventional photon therapy where the photon beam is shaped by collimators and absorbers. The energy modulation of charged particle beams was first performed with modified collimator and absorber techniques [Chu 1993]. Although these techniques did not exploit the possibilities of charged particles to a maximum, dose distributions could be reached that were superior to those of photon therapy of that time. Especially the dose increase towards the end of the particle range produced doses that are higher in the target than in the entrance channel. In addition, the fast fall off of dose beyond the Bragg maximum allows field geometries never possible with electromagnetic radiation. These treatments were performed at particle accelerators that had originally been built for nuclear physics experiments and were then adapted to tumor therapy. This was the case in Berkeley, where proton and ion treatment started, as well as in Harvard proton cyclotron where up to now the highest number of patients have been treated successfully.

Dedicated therapy units went into operation first at Loma Linda, California, where now about one thousand patients are treated with protonsper year. At Chiba in Japan, the first heavy-ion therapy unit was completed in 1984 and is dedicated to medical purposes alone. An important improvement at the Loma Linda facility was achieved with the construction of mobile beam delivery systems, gantries that allow to irradiate the patient from any angle.

The first place, where gantry and tumor-conformal treatment using a 1-dimensional beam scanning was combined, was the experimental therapy at PSI, Villigen, Switzerland. 2-dimensional scanning combined with active energy variation but without gantry was first used in patient treatment with carbon ions at GSI, Darmstadt, Germany. A complete list of former and present therapy units is given in Tab. I together with the starting date of patient treatment as well as the number of patients treated until December 1999.

The vast majority of the altogether nearly 31,000 patients were treated with protons and only a few hundred with heavier ions like neon or carbon. Because of their increased relative biological effectiveness (RBE) ions heavier than protons are called "heavy ions" in radiobiology although they are light ions compared to the terminology used in nuclear physics. The main reason for an elevated RBE is the increase in ionization density in the individual tracks of the heavy particles, where DNA damage becomes clustered and therefore more difficult to repair [Kraft 1997].

Tab. I: **WORLD WIDE CHARGED PARTICLE PATIENT TOTALS**
[Sisterson 2000]

January 2000

WHO	**WHERE**	**WHAT**	**DATE FIRST RX**	**DATE LAST RX**	**RECENT PATIENT TOTAL**	**DATE OF TOTAL**
Berkeley 184	CA. USA	p	1954	— 1957	30	
Berkeley	CA. USA	He	1957	— 1992	2054	June-91
Uppsala	Sweden	p	1957	— 1976	73	
Harvard	MA. USA	p	1961		8372	Dec-99
Dubna	Russia	p	1967	— 1974	84	
Moscow	Russia	p	1969		3100	Dec-98
St. Petersburg	Russia	p	1975		1029	Jun-98
Berkeley	CA. USA	heavy ion	1975	— 1992	433	June-91
Chiba	Japan	p	1979		96	Oct-96
PMRC, Tsukuba	Japan	p	1983		629	July-99
PSI (72 MeV)	Switzerland	p	1984		3014	Dec-99
Dubna	Russia	p	1987		43	Dec-99
Uppsala	Sweden	p	1989		215	Oct-99
Clatterbridge	England	p	1989		960	Dec-99
Loma Linda	CA. USA	p	1990		4726	Dec-99
Louvain-la-Neuve	Belgium	p	1991	— 1993	21	
Nice	France	p	1991		1350	Jun-99
Orsay	France	p	1991		1522	Sept-99
N.A.C.	South Africa	p	1993		341	Dec-99
MPRI	IN USA	p	1993		34	Dec-99
UCSF - CNL	CA USA	p	1994		246	Dec-99
HIMAC, Chiba	Japan	heavy ion	1994		473	Sept-98
TRIUMF	Canada	p	1995		55	Dec-99
PSI (200 MeV)	Switzerland	p	1996		41	Dec-99
GSI Darmstadt	Germany	heavy ion	1997		57	Mai-00
HMI Berlin	Germany	p	1998		105	Dec-99
NCC, Kashiwa	Japan	p	1998		18	Dec-99

For carbon ions the strongly elevated RBE region is restricted to the end of the particle range while in the entrance channel DNA damage predominates that can be repaired. For heavier ions like neon the irreparable damage becomes more important in the entrance channel, too (Fig. 2). However, because RBE depends on the possibility to repair the damage produced in the DNA, the repair capacity of the irradiated tissue becomes relevant. In general, slowly growing tumors have a great repair capacity and are normally very radioresistant. For ion treatment they show the greatest increase in RBE. This is why these tumors are most appropriate for a therapy with carbon ions.

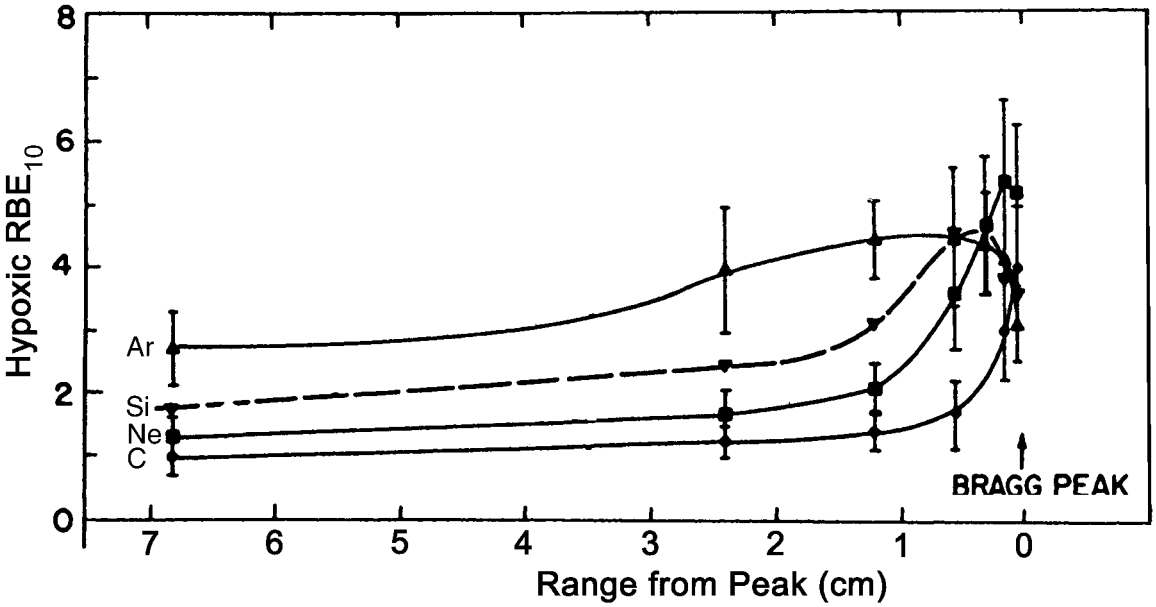

Fig. 2: RBE for C, Ne, Si and Ar ions as function of the penetration depth [redrawn from Blakely 1980]

In addition to the greater RBE, carbon ion beams also have a smaller lateral scattering and range straggling [Blakely 1994, Tobias 1979]. This is an improvement of the dose distribution when compared to protons but also when compared to the most modern techniques of photon irradiation. Another plus of the carbon ions represents the small amount of nuclear fragmentation of the projectile ion. This is frequently seen as a drawback compared to proton irradiation because it produces a small tail of dose beyond the Bragg maximum consisting of protons and other light ions. But the major advantage is the production of positron emitting carbon isotopes ^{10}C and ^{11}C that can be measured from outside by the coincident registration of the annihilation quanta. Using this modified positron emission tomography (PET) the distribution of the positron emitters and consequently of the primary carbon ions can be monitored and compared to the planned distribution [Enghardt 1999].

Because of the increased RBE, the improved dose distribution and the possibility of PET monitoring, carbon treatment exceeds the possibilities of protons in therapy considerably [in: Groß 1998]. But these advantages have to be paid for by some restrictions: carbon therapy is more expensive and has to be better controlled than the less sensitive proton therapy. Because of the higher magnetic rigidity and greater energies, the heavy-ion accelerators are more expensive and beam transport lines require larger magnets. Up to now, no heavy-ion gantry has been realized because of its large dimensions and the problem of its mechanic stability. Consequently, alternatives for the beam distribution from different angles have to be considered. In addition, the quality assurance and the beam control has to be more stringent in order to guarantee precise irradiation. Last but not least, treatment planning has to reach a much higher level of sophistication: first, it must be guaranteed that the very efficient part of the beam that corresponds to the elevated RBE is strictly confined to the target volume. Secondly, the correction of the physical dose by the appropriate RBE requires a treatment planning that includes the RBE dependence on particle energy

and atomic number as well as on dose and tissue for the complete irradiation field. Because heavy ions are more effective in the production of biological damage than protons, they can improve the control of radioresistant tumors but their application has to be performed extremely careful.

II THE PHYSICAL BASIS OF ION BEAM THERAPY

The main arguments for the use of particle beams in therapy was - from the beginning – the inverse depth dose profile i.e. the increase of energy deposition with penetration depth. The increase of ionization density with range was first described for α-particles in a publication by Bragg in 1903 and was confirmed for protons and heavier ions in measurements by Robert Wilson at Berkeley, California, in 1946 [Wilson 1946].

In Fig. 1 the depth dose profile of electromagnetic radiation is compared to that of carbon ions. For low-energy X-rays the stochastic absorption by photo and Compton processes yield an exponential decay of absorbed dose with penetration. For greater photon energies the produced Compton electrons are strongly forwardly scattered and transport some of the transferred energy from the surface to greater depth yielding an increase in dose in the first few centimeters. For high-energy electron Bremsstrahlung, that is mostly used in conventional therapy, this maximum is shifted in a few centimeters from the surface of the patient's body sparing the very radio-sensitive skin. In addition, the exponential decay becomes less steep improving the ratio of entrance dose to target dose for the treatment of deep-seated tumors.

In contrast, the energy deposition of heavy charged particles like protons or heavier ions increases with penetration depth and reaches a maximum (Bragg peak) just before the end of the range. This behavior is due to the dependence of the energy loss on the particle energy (Fig. 3).

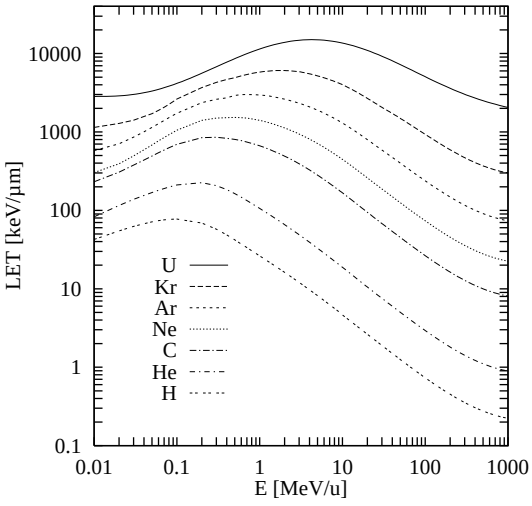

Fig. 3: Energy loss of different particles as function of the energy, calculated with ATIMA [Schwab 1991].

Within the range of therapeutically relevant energies of several hundred MeV/u the process of energy loss is dominated by electronic collisions and can be described by the Bethe-Bloch-formula [Bethe 1930, Bloch 1933a, Bloch 1933b]:

$$\frac{dE}{dx} = \frac{4\pi e^4 Z_{eff}{}^2 ZN}{m_e \upsilon^2} \ln \frac{2m\upsilon^2}{I} + \text{relativistic terms}$$

(equ.1)

with $\frac{dE}{dx}$ energy loss per length, Z the target atomic number, N the electron density of the target, m_e and e the mass and charge of the electron, υ = ßc the projectile velocity. The effective projectile charge Z_{eff} is shown in fig. 4. It can be approximated by the Barkas formula [Barkas 1963]:

$$Z_{eff} = Z(1-\exp-125\beta Z^{-\frac{2}{3}}) \qquad \text{(equ.2)}$$

The dominant part in the Bethe-Bloch-formula is the $\frac{1}{\upsilon^2}$ and the Z_{eff} dependence. The $\frac{1}{\upsilon^2} \approx \frac{1}{E}$ dependence yields an increase in energy loss with decreasing particle energy. At low energies electrons are collected from the target and Z_{eff} in the nominator decreases rapidly yielding a distinct maximum of energy loss at low energies [Bohr 1913]. When the energy loss is plotted over the penetration depth its maximum is located at the end of the track. The low-energy loss at higher energies yields a nearly constant plateau of energy deposition in the entrance channel.

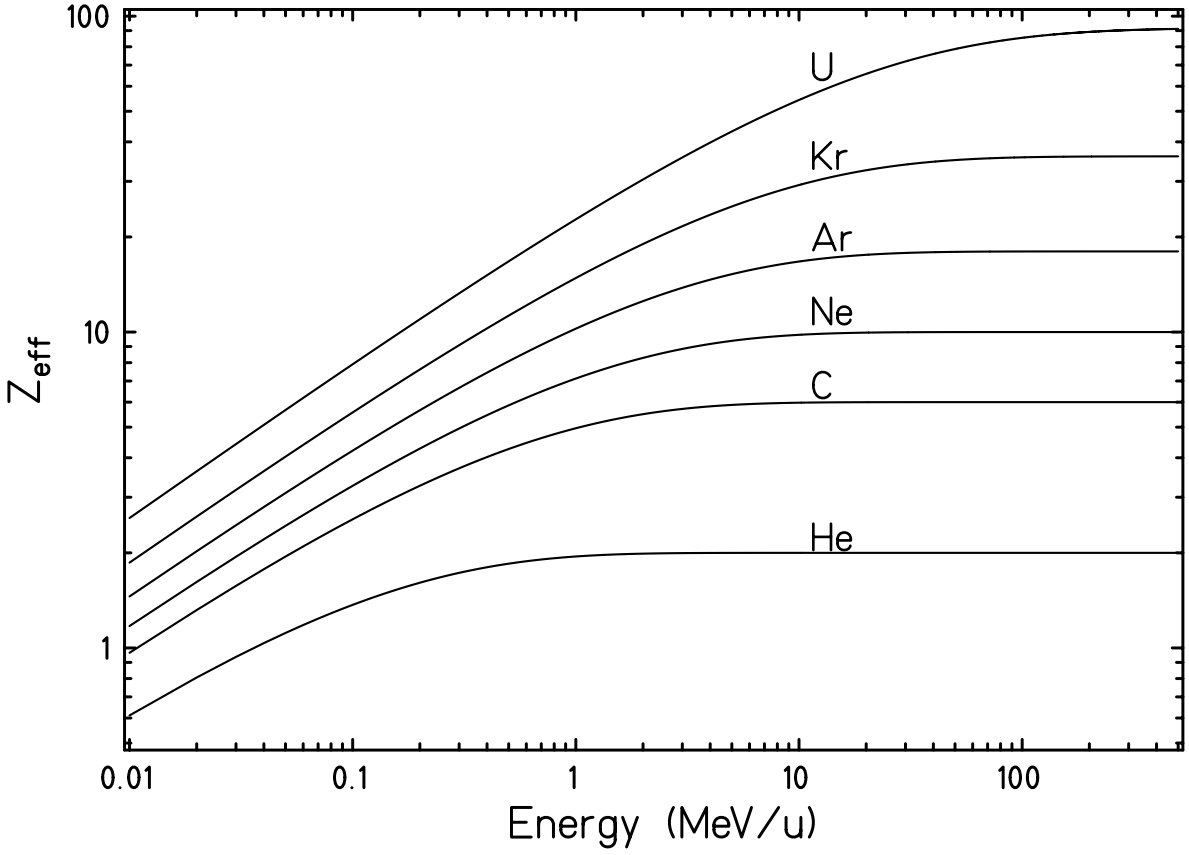

Fig. 4: Z_{eff} as function of particle energy. With increasing particle energy more electrons are stripped off and Z_{eff} appraoches the atomic number Z.

For a single particle, the maximum of its energy loss is much sharper according to the Bethe formula than the Bragg curve of a beam measured in an ionization chamber. The width of the measured Bragg curve is caused by the residuum of multiple scattering processes that yield an almost Gaussian energy loss distribution f (ΔE) [Bohr 1915, Ahlen 1980]:

$$f(\Delta E) = \frac{1}{\sqrt{2\pi\sigma}} \exp \frac{(\Delta E - \langle \Delta E \rangle)^2}{2\sigma^2}$$

with

$$\sigma^2 = 4\pi Z_{eff}{}^2 Z_2 N \Delta x \left(\frac{1-\beta^2/2}{1-\beta^2} \right)$$

(equ.3)

An additional energy loss straggling is also found at very low particle energies because of the straggling of Z_{eff} by electron loss and capture i.e. charge changing processes [Geissel 1982]. But the charge changing straggling occurs only at very low energies and does not contribute significantly to the width of the Bragg curves. Because the width depends on the penetration depth Δx of the particles, for greater particle energies and longer penetration the half width of the Bragg maximum becomes larger and the height smaller. Typical values for carbon ions are given in Tab. II [Weber 1996].

Tab. II: Typical values for carbon ions

Energy [MeV/u]	90	198	270	330
Range [mm]	16.1	76	133.5	186.5
straggling FWHM [mm]	0.7	2.3	5.0	7.0

The values of the width of the Bragg maximum determines the gradient of the distal fall-off of the dose distributions. For a typical tumor treatment in the head, ranges of 10 cm are used that correspond to a FWHM of 4 - 5 mm or a gradient of half of this value which is very good. However, in practice, range profiles are determined rather by the density distribution of the penetrated tissue than by the intrinsic straggling.

For smaller penetration depths, frequently the half width of the Bragg maximum has to be increased artificially: in active scanning, the beam delivery to the target volume is dissected into slices of equal particle range in the distance of the width of the Bragg maximum. If the Bragg maximum is too sharp, too many slices are needed to fill the complete target volume. In this case it can be very advantageous to enlarge the Bragg maximum by a passive absorber system to 2-3 mm in order to reduce the overall treatment time [Weber 1999].

Lateral Scattering

For the clinical application, the lateral scattering of the beam is more important than the longitudinal. Because of possible range incertainties the treatment planning will avoid a beam directly stopping in front of a critical structure. Therefore, tumor volumes close to critical structures can only be irradiated with the beam passing by. How close the beam can get is consequently determined by the lateral scattering.

Lateral scattering mainly results from Coulomb interaction of the projectiles with the target nuclei. But also the kinematic of nuclear reactions contributes to the lateral width of a beam, predominantly at the distal side of the Bragg peak where the primary projectiles are stopped and the residual dose is made up of contributions of nuclear fragments only [Weber 1999]. The Coulomb scattering of the projectiles is described very precisely in the theory of Molière [Molière 1948]. Measurements of

proton scattering [Gottschalk 1992] confirmed this theory and a parametrization [Highland 1975] for small angle scattering having an angular distribution f(α):

$$f(\alpha) = \frac{1}{\sqrt{2\pi\sigma_\alpha}} \exp\left(-\frac{\alpha^2}{2\sigma_\alpha}\right)$$

$$\sigma_\alpha = \frac{14.1MeV}{\beta pc} Z_p \sqrt{\frac{d}{L_{rad}}\left(1+\frac{1}{9}\log_{10}\frac{d}{L_{rad}}\right)}$$

(equ.4)

Where σ_α is the standard deviation, p the momentum, L_{rad} the radiation length and d the thickness of the material.

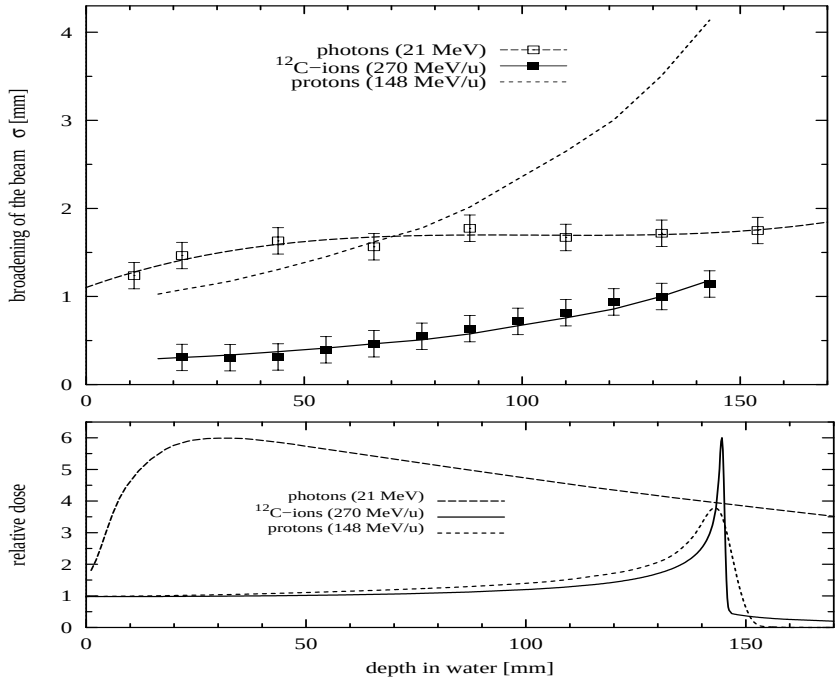

Fig. 5: Comparison of the lateral scattering of photon, proton and carbon beams as function of the penetration depth (top) and the depth dose correlation (bottom) [Weber 1996].

In figure 5 the lateral scattering of a therapy beam is compared for 21 MeV photons, for protons and carbon ions of a range of 14.5 cm in water. The comparison shows very clearly that for protons the lateral scattering exceeds the photon value for penetration depth larger than 7 cm. The lateral deflection of carbon beams is better than 1 mm up to a penetration depth of 20 cm

Dose of an Ion Beam

In radiobiology and therapy the absorbed dose is defined as the energy deposited per mass unit [ICRU 1970]. By definition 1 Gray corresponds to 1 Joule per kilogram. If a thin volume – thin compared to changes in the energy loss of a particle – is irradiated by a parallel beam of particles the dose in Gray in this volume is given as

$$D[Gy] = 1.6\times10^{-9} \frac{dE}{dx}\left[keV/\mu m\right] \times F\left[cm^{-2}\right] \times \frac{1}{\rho}\left[\frac{cm^3}{g}\right]$$

(equ.5)

where $\frac{dE}{dx}$ is the energy loss, ρ the density of the stopping material and F the particle fluence i.e. the number of primary ions traversing the unit area.

In radiotherapy the energy of the primary particle has to be varied in order to fill the target volume with a homogeneous dose or to produce a homogeneous biological effect. Therefore, the particle field contains particles of different energies. In addition, heavy projectiles are fragmented by nuclear disintegration producing ions of all atomic numbers below that of the projectile. Then the dose has to be calculated as the energy loss of the respective particles integrated over the different atomic numbers and energies.

In principle, it is possible to calculate the dose distribution for each beam and then to add up the various dose contributions to each volume element. For a dose optimization based on absorbed dose only this procedure is sufficient and is usually done for protons where RBE does not play a major role. But for heavy ions the biological response critically depends on particle energy and atomic number. The relative biological effectiveness (RBE) can first increase by a factor of 2 to 4 when heavy particles are slowed down and then decrease to values below 1 [Kraft 1997]. Consequently, the composition of a complex particle field has to be known for heavy ion therapy when variations of RBE have to be included in the dose optimization. Similar variations in effectiveness are also found for the response of solid state radiation detectors like films or thermoluminescent detectors [Geiß 1998, Bathelt 2000] . In these detectors, the high ionization density at the end of the particle range yields saturation effects that deteriorate the measured signal. Therefore, for dosimetry as well as for therapy planning it is essential to know the composition of the radiation field regarding energy and atomic number.

Nuclear Fragmentation

When a particle beam of carbon ions penetrates a thick absorber a small amount of the primary beam will undergo nuclear fragmentation. Because these nuclear reactions take place mostly at higher energies of several hundred MeV/u they can be approximated in a two step process. First, the collision that takes about 10^{-23} sec and generates partially excited prefragments and secondly, the de-excitation by nucleon evaporation and the emission of photons, forming the final number and size of fragments, that takes 10^{-21} to 10^{-16} sec. Without going into a detailed review of the different model calculations [Friedländer 1985, Hüfner 1985] some common conclusions can be drawn that are relevant for therapy.

Because of the high energy, geometrical factors are important and according to geometry peripherical collisions are by far more frequent than central collisions. The peripheral collisions produce only a partial overlap between projectile and target nuclei. Consequently, the projectile fragments remain large and travel with almost the same velocity in a forward direction. Multi-fragmentation i.e. the blow-up of the reaction partners into many fragments is rather rare. Because of the rather slow transition of pre-fragments to fragments, selection rules play a significant role and the abundance of the different fragments is not monotonously decreasing in atomic number. Because of the nearly unperturbed velocity of the fragments, the secondary fragmentation cannot be neglected and has to be taken into account for thick absorbers. Finally, because of the reaction kinematics the emission angle of the fragments is larger than the lateral scattering of the primary beam by multiple electronic scattering and the fragment tail behind the Bragg peak has a larger width.

In order to produce the accuracy that is indispensable for treatment planning, the parametrization of the fragmentation process has to rely on measured fragmentation data rather than on theoretical

values. For neon ions, as used in Berkeley, the fragmentation was measured by Schimmerling et al [Schimmerling 1989]. For carbon ions, Sihver et al. [Sihver 1998] have measured fragmentation as well as Schall et al. [Schall 1996].

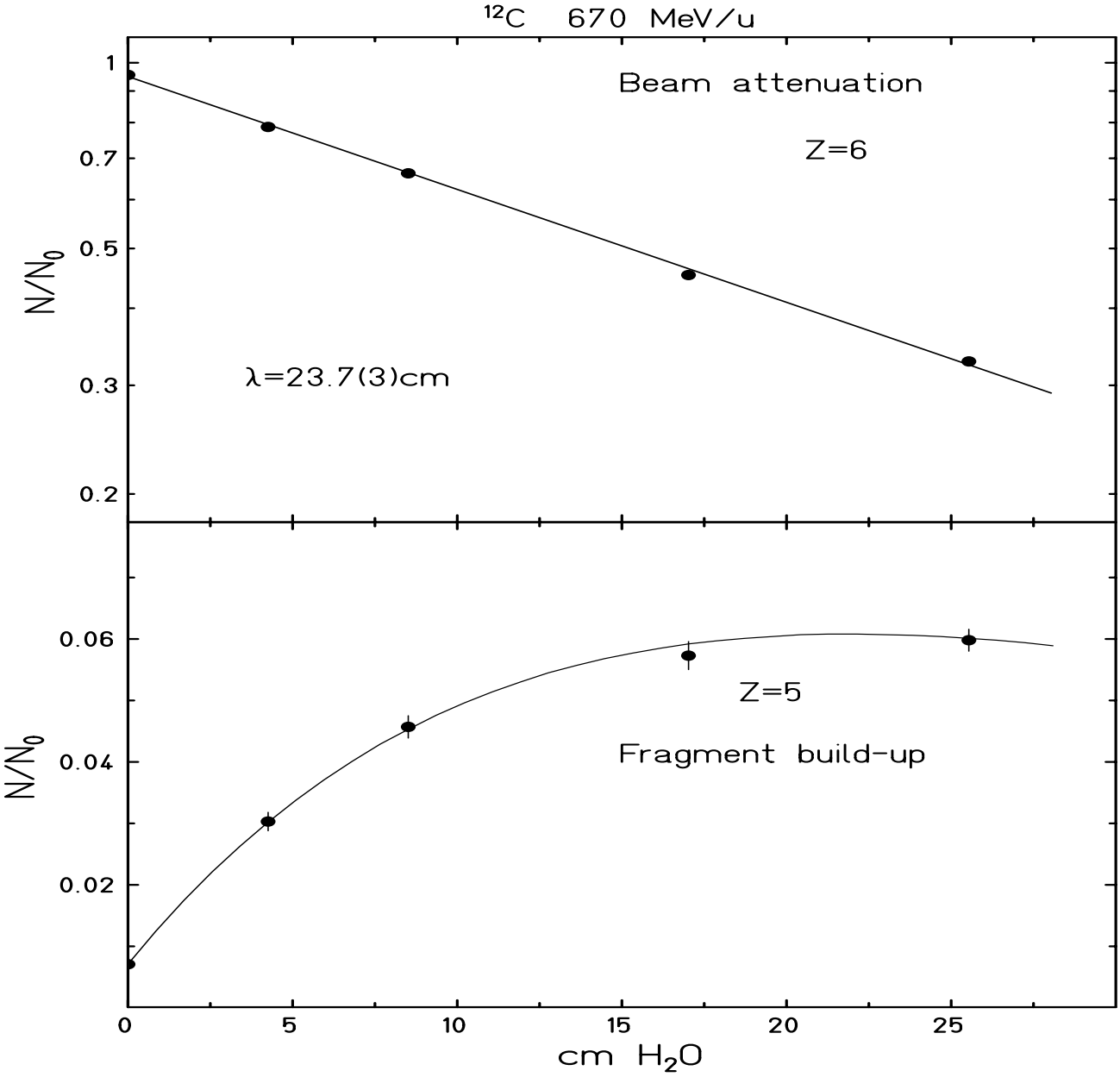

Fig. 6. Fragmentation of a 670 MeV/u carbon beam in water [Schall 1994]. Top: attenuation of the primary carbon beam as function of the penetration depth yielding a mean free path length λ = 23,7 cm. Bottom: Build up of Boron ion fragments. Because of further fragmentation to lighter ions the intensity of Boron levels off for larger penetration depths. [Schall 1996]

In Fig. 6 the attenuation of the primary carbon beam (top) and the built-up of B-ions is given as function of the penetration depth. In Fig. 7 the Bragg curve is separated into dose contribution from the primary beam and from first and second generation of fragments. Evidently, the dose of the fragments has to be included into the dose calculation in treatment planning, especially for a correct description of the fragment tail beyond the Bragg maximum. Another problem is the wider angular distribution of the fragments than of the primary beam that has to be included in 3-dimensional beam models [Golovkov 1997].

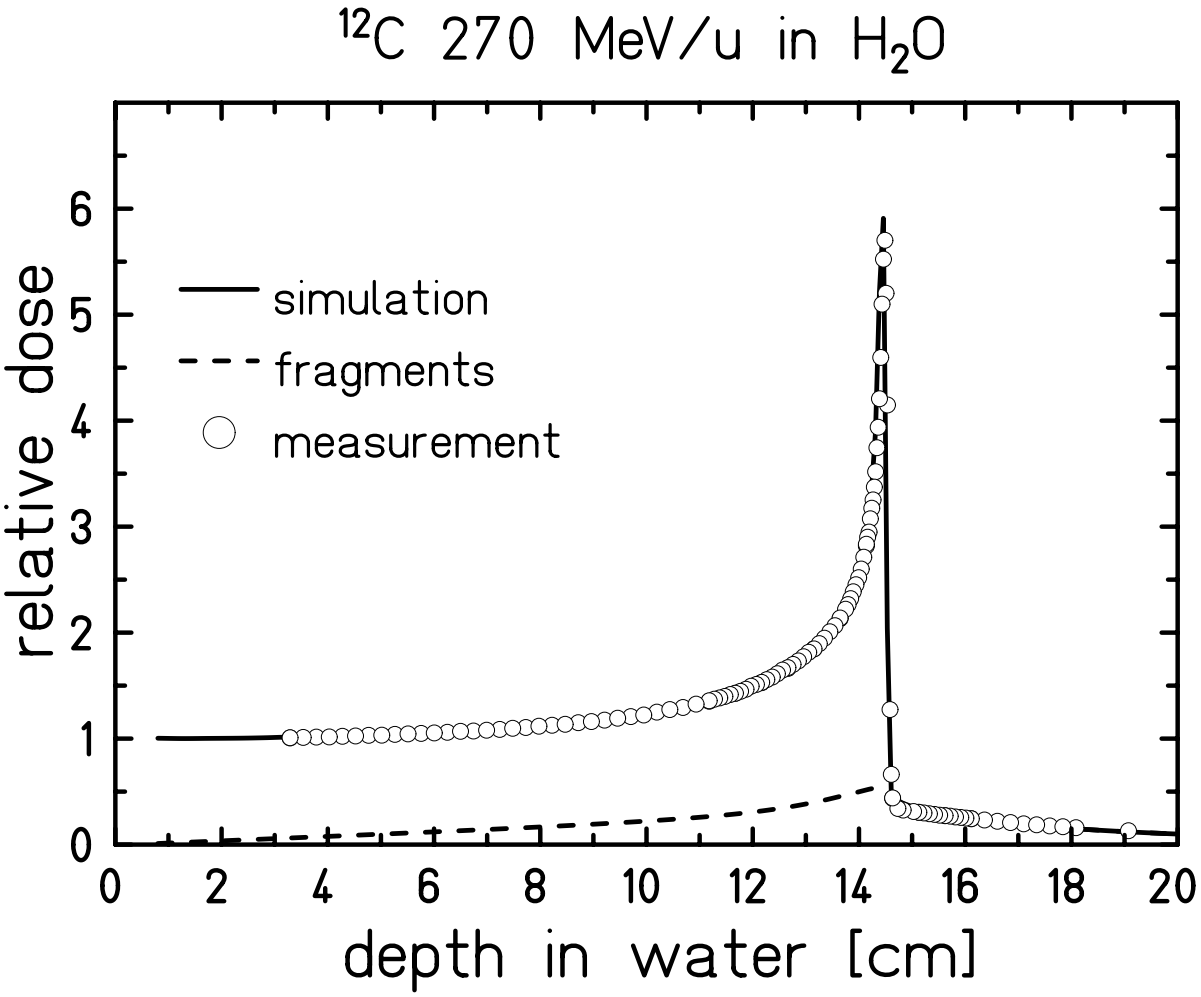

Fig. 7: Bragg curve of 270 MeV/u carbon ion Measurements are compared with calculations including the contribution from nuclear fragments

In general, beam fragmentation tends to deteriorate the sharp dose contours by enhanced lateral and longitudinal scattering. This is a minor problem at the high energies in the entrance channel but becomes more important at the tail of lighter fragments beyond the Bragg maximum. Fragmentation restricts the use of material in the beam, especially in cases when the beam energy is varied to a large extent by the insertion of absorber material. In particular for heavier ions like neon an intolerable amount of fragments is produced. For carbon ions the amount of fragmentation stays in a tolerable limit when the beam energy is adjusted by the accelerator and no passive beam shaping devices are used.

Production of Positron-Emitting Isotopes

All the possible drawbacks originating from beam fragmentation are more than compensated by the possibility of the *in-situ* beam observation using positron emission tomography (PET). A very frequent process of fragmentation is the stripping of one or two neutrons, converting the stable ^{12}C isotope into the positron-emitting isotopes ^{11}C and ^{10}C that decay with half-lives of 20 min and 19 sec, respectively [Enghardt 1992].

Because the loss of one or two neutrons causes only small perturbations these isotopes continue to travel with the almost same velocity to almost the same range. The range relation between the higher carbon fragments and the stable primary isotope is given approximately:

$$R \approx \frac{A}{Z^2} \qquad R(^{11}C) = R(^{12}C) \times \frac{11}{12}$$

(equ.6)

Therefore, the measurement of the coincident emission of the two annihilation gamma quanta with an appropriate gamma camera can be used to trace back the stopping points of the carbon ions. In Fig. 8 the distribution of beta decays is given as function of penetration depth. The two peaks of ^{10}C and ^{11}C are clearly visible and in addition, the background from target activation, mostly ^{15}O isotopes, can also be seen. The PET analysis of a primarily stable beam that becomes contaminated by $ß^+$ isotopes – the so-called "auto-activation" [Tobias 1977, Enghardt 1992] – represents a powerful tool for the visualization of the particle distribution inside the patient's body in the course of the treatment. It is an alternative to the frequently proposed treatment with a radioactive beam [Bimbot 1999].

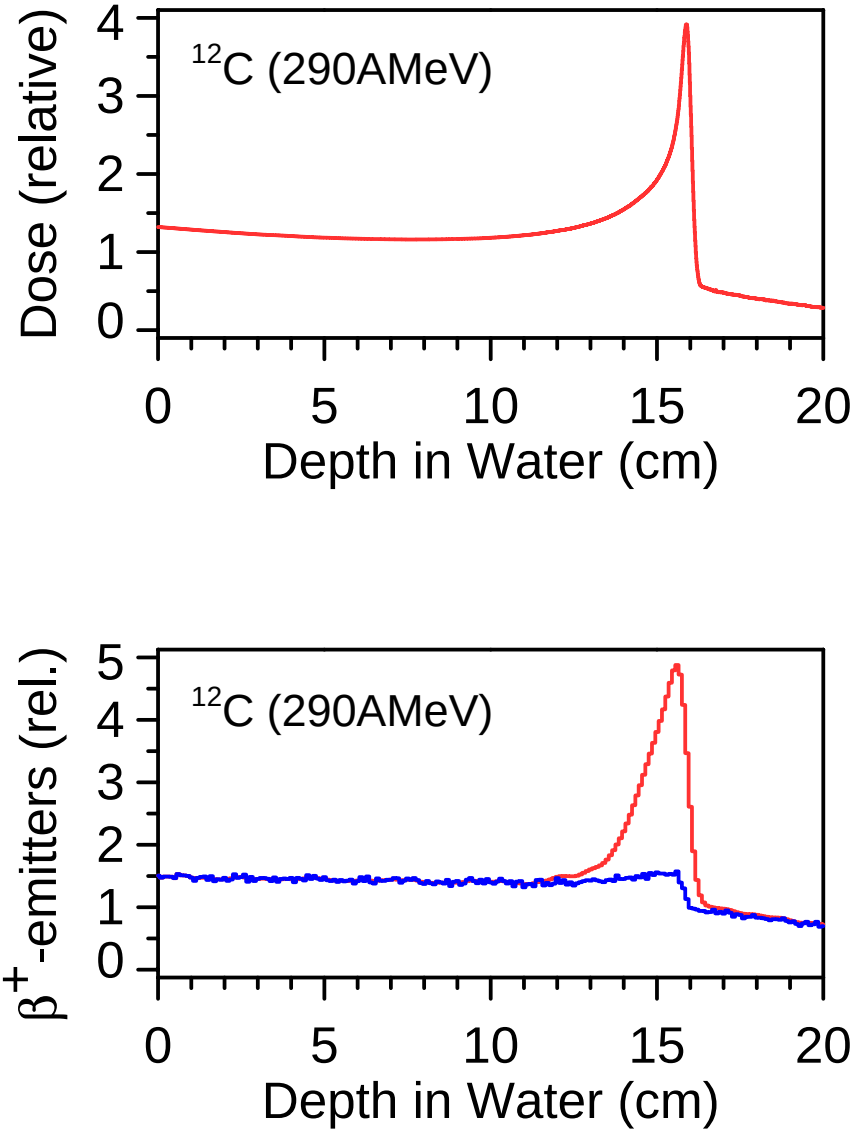

Fig. 8: The Bragg curve (top) is compared to a calculated $ß^+$ distribution expected for the irradiation of a PMMA absorber with a monoenergetic carbon ion beam. Bottom: the upper line displays the projectile fragments and the lower line the target fragments (with the courtesy of W. Enghardt).

The treatment with a radioactive beam like that of ^{11}C isotopes would generate problems of another kind. The production of these isotopes after acceleration requires a 100 times larger beam intensity and a sophisticated and expensive fragment separator in front of the treatment beam line. The

treatment with a radioactive beam does not increase the biological effectiveness in the target volume because the beta decay energy of a few keV does not add a significant portion of dose to the total dose released by the primary beam.

Auto-activation instead is a very clean and reasonable method to make use of the unavoidable beam fragmentation. However, the cross sections are low and consequently the counting rate is not high. 30,000 to 50,000 coincidences are measured in the GSI-version of PET cameras when treating an average volume of 100 to 200 cm^3 in the head with a dose of 3 Gye. Because of this low coincidence rate the contamination with accidental coincidences has to be kept low and any source of radioactivity –such as contaminated collimators or absorbers – have to be avoided. It has been found that the carbon activity is washed out from soft tissue with a half life of 100 sec presumably as CO_2 in the blood flow [Chatterjee 1976; Tomitani 1999].

With kinetic factors like the different decay times and the wash-out effect it is possible to reconstruct the location of the beam's particles stopping. The use of on-line PET for beam localization is one of the great advantages of an irradiation with carbon ions. This allows to treat tumors adjacent to critical structures with a high intensity beam. PET analysis, however, does not allow an on-line control of the beam in its application. Only after a fraction has been applied the results of irradiation can be compared to the intended distribution. In case of discrepancies the treatment plan for the next fraction can be altered. Comparisons of PET measurements with treatment plans will be given further down.

Microscopic Structure of Ion Beams

The fact that dose i.e. the energy deposition of heavy charged particles has to be corrected by the relative biological effectiveness (RBE) indicates that not only the energy deposition but also the internal structure of the particle tracks are important for the biological response as well as for the response of detectors, like films, semiconductors or thermoluminescent detectors. The formation of a particle track can be regarded as a two-step process: first the emission of electrons by the ion impact and second the transport of theses electrons through the material around the particle track, causing secondary ionization and energy deposition.

The calculation of track structure has been the subject of many publications in which different approaches have been examined. Two main groups can be distinguished. The first are analytical or semi-empirical models like those of Chatterjee or Butts [Chatterjee 1976, Butts 1967] who use simplified assumptions of electron energy and angular distributions to obtain analytical descriptions of the radial dose distribution. The models of the second type treat energy and angular distribution of primary and secondary electrons in detail by Monte Carlo (MC) simulation where each basic interaction is treated individually [Wilson 1999, Paretzke 1987, Krämer 1994 and others].

Although the various models vastly differ in their basic assumptions and their input data, the obtained radial dose distributions are very similar. Over a large range of radial distances the dose falls off like $\frac{1}{r^2}$ with the exception of the region r < 10 nm and distances close to the maximum track radius (Fig. 9). Whereas the analytical models have the advantage of being easily understood and easy to calculate one of their disadvantages is that the $\frac{1}{r^2}$ distributions diverges at r = 0. Hence some cut-off procedures have to be introduced to obtain finite dose values for very low distances. This is not necessary for the MC-type models since they follow the reality of energy deposition more closely.

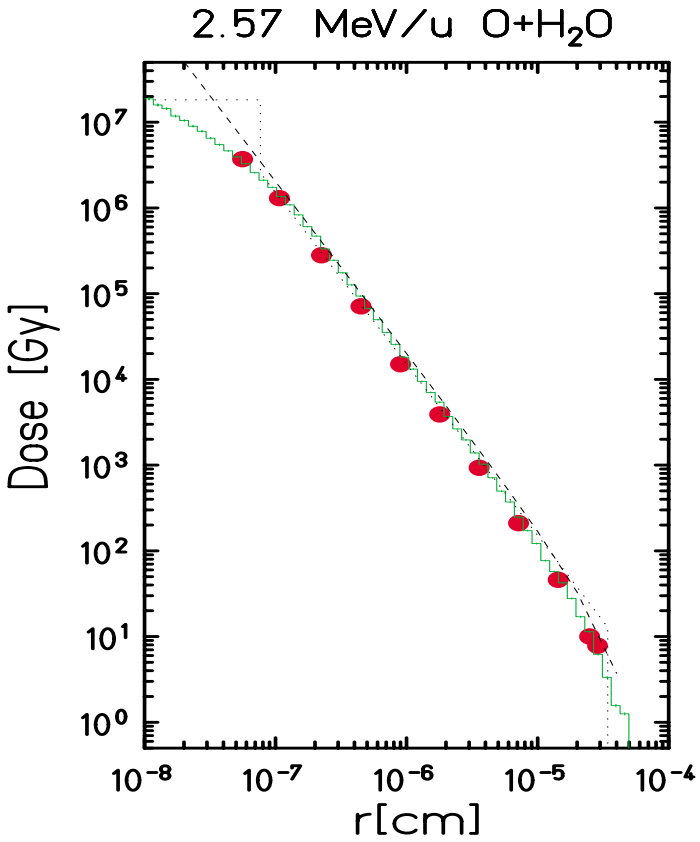

Fig. 9: Radial dose distribution inside a particle track according to different calculations are compared to measurements [Krämer 1994]

In general, the energy released by the primary ions is distributed over the volume of the track with a steep gradiant of local dose over many orders of magnitude, from milli-Grays at the maximum track radius to mega-Grays in the center. In order to elucidate the consequences of such an inhomogeneous dose distribution for the biological effectiveness the physical basis of the track formation like electron emission and transport will be discussed in the following. It is, however, beyond the scope of this paper to go into details of the various track calculations. We refer to recent articles [Cucinotta 1999, Kraft 1999 b].

Electron Emission in Ion-Atom Collisions

When passing through an absorber, swift ions strip off all electrons having an orbital velocity smaller than the projectile velocity [Bohr 1948]. This causes an increase in the effective charge Z_{eff} with higher velocities that can be approximated by the Barkas formula [Barkas 1963]. Light ions like carbon are fully stripped off their electrons at energies necessary for therapy. The main interaction of these bare nuclei with the target is the collision with the target electrons. Because of the large mass difference between carbon nuclei and electrons the center of mass system coincides with the projectile mass

$$E_{cm} = \frac{m_p}{m_p + m_e} E_{projectile} \approx E_{projectile} \qquad \text{(equ.6)}$$

and electrons scattered in the center of mass system are emitted symmetrically to the projectile. In Fig. 10a a velocity coordinate system is given. The velocity relative to the center of mass system and the projectile velocity can be added to the laboratory velocity. In Fig. 10b a measured electron distribution is given in the same reference coordinates. The most prominent structure is the emission around the projectile that corresponds to the collision of the heavy projectile with a quasi

free electron – the so-called binary encounter - BE: Neglecting the binding, the BE electrons should be emitted in the laboratory system with an energy $E_e = 4\frac{m_e}{m_p}\cos^2\vartheta \; E_p$. If the electrons were at zero energy before the collision, then strict binary encounter kinematics would yield one electron energy for each scattering angle. The electron energy distribution before the scattering as given by the Compton profile produces the observed broad structure around the center of mass.

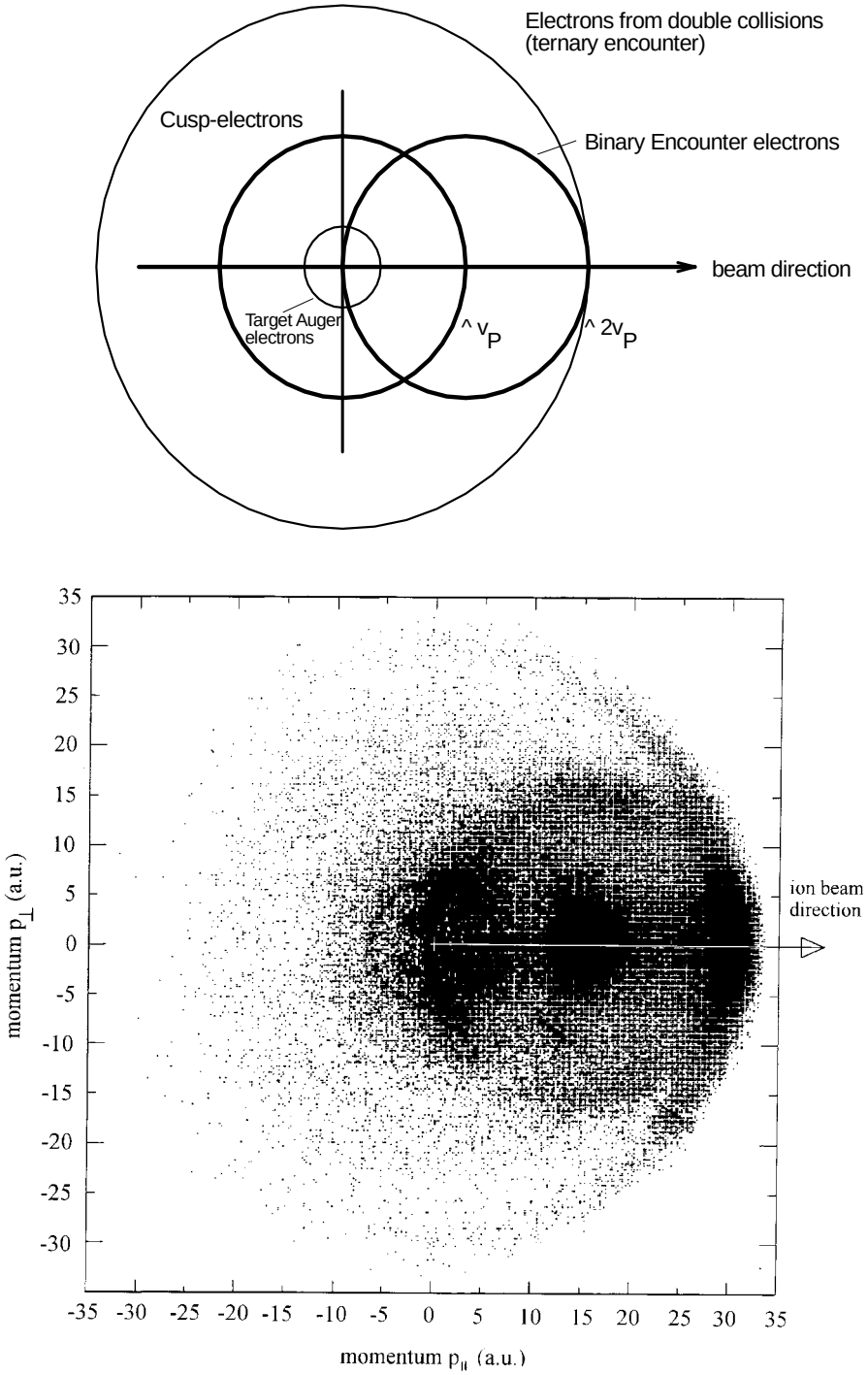

Fig. 10: Top: Velocity coordinates of the electron emission in ion-atom collisions.
Bottom: Angular distribution of the measured electron emission. [Reinold 1998]

The second-most important electron emission is found at the center of mass i.e. electrons travelling with the speed of projectiles in a forward direction. These electrons are called convoy electrons because they correspond to the charge exchange of the projectile where electrons are picked up and

lost by the projectile. Finally, a peak of electrons is also found at very small velocities which are liberated in distal collisions having small energy transfers where the binding of the target atoms is not negligible.

The main feature of the electron emission pattern for track formation is the strong forward emission of electrons having velocities up twice the projectile velocity. Although emitted in forward direction it is the range of these electrons that determines the diameter of the particle track because the original angular distribution is very quickly washed out by multiple scattering. The very fast loss of angular orientation after a few collisions is the main reason why models using incorrect angular distributions of electron emission yield comparable radial dose distributions as models starting with the measured forward peaked distributions. The same is true to some extent for the shape of the electron energy spectrum: sharp structures like Auger electrons are not important because they are washed out after a few collisions. Only the general shape of the spectrum i.e. the ratio of low to high energy electrons is important. This is the reason why many different approaches starting from very different data predict similar radial dose profiles.
It has to be noted that the electron emission experiments are mostly performed with gas targets under single collision conditions. For a solid target multiple collisions of the outgoing electrons are expected as well as screening effects of the distant collisions that would reduce the intensity at the low-energy part of the spectrum. Hence the accuracy of dose calculation in the track center might be affected by the different primary-electron distribution in condensed phase.

Electron Transport

The major part of the energy loss of the primary ions is transformed into kinetic energy of the emitted electrons [Groeneveld 1979]. Consequently, the action of these electrons determines the biological response together with the primary ionization. It was and is a frequently discussed question whether the interaction events – the so-called biological lesions - caused by density ionizing particle irradiation would be of a different character than for irradiation by sparsely ionizing radiation and whether these physical differences could directly be correlated to the differences in the radiobiological response.
According to the classical theory of microdosimetry an event was originally defined as the total energy deposition in a volume of $1\mu m^3$ of tissue equivalent density [Kellerer 1987]. In gas of low density these volumes of cubic micrometers are blown up to dimensions of centimeters and allow to measure event distributions using ionization chambers. Although these distributions did show significant differences when the radiation quality was changed it was not possible to use the event distribution to calculate the biological response directly. However, most of what we presently know about radial dose distribution originates from these measurements [Varma 1980, Toburen 1980].

The electron transport is governed by the elastic and inelastic collision cross sections that originate from different excitation and ionization processes. Comprehensive reviews of this subject were given by Märk 1995, Sanch 1995 and Paretzke 1988. The cross sections for electron collisions in water vapor as tissue equivalent can also be taken from experiments. Fig. 11 depicts the cross sections for elastic scattering, excitation and ionization as function of electron energy. These relations are not very different when using another target consisting of light elements only like DNA. The elastic cross section dominates at small electron energies where ionization is not possible because of the binding energy as a threshold. When the electron energy exceeds the binding energy the ionization cross section is rapidly increasing and reaches a maximum at about 100 eV. The shape of this maximum and its energy location are widely independent from the atomic conditions of the target and are expected to be the same on the intracellular level.